THERMOSPHERIC NITRIC OXIDE AND ITS ROLE IN THERMOSPHERIC DYNAMICS AND COMPOSITION

J-Cl. Gerard
Institut d'Astrophysique, Universite de Liége - B4200 Cointe-Liége Belgium
and
R. G. Roble
National Center for Atmospheric Research - P.O. Box 3000 - Boulder Colorado 80307

The global distribution of thermospheric nitric oxide has been measured under different geophysical conditions by the Atmosphere Explorer (AE) and Solar Mesosphere Explorer (SME) satellites. These observations show a great variability in the NO concentration but the existence of a latitudinal gradient is clearly evidenced by statistical maps of the NO meridional distribution. A two-dimensional zonally averaged chemical-dynamical model has been used to investigate the importance of nitric oxide 5.3 μm cooling and its role on thermospheric temperature, dynamics and major gas composition.

For this purpose, a 2-D background atmosphere code and an odd nitrogen code have been coupled and run to steady state. The NO distribution obtained is in good agreement with the AE-D global picture calculated at solstice for solar minimum activity. The importance of each term in the thermodynamic equation has been studied spatially. It is found that the NO I.R. cooling term competes with conduction in the upper thermosphere and reaches its maximum value near 200km at high summer latitudes.

The primary effect of including the NO cooling term is to increase the temperature in the upper winter thermosphere and decrease it in the other hemisphere, if the global average temperature is fixed. In general, the strength of the circulation is decreased and the thermal gradient is smoother. As a consequence of these changes in the wind and temperature fields, the O_2, N_2 and O densities also react to the effect of the NO cooling. The importance of this process depends on the level of solar activity which controls the NO distribution.

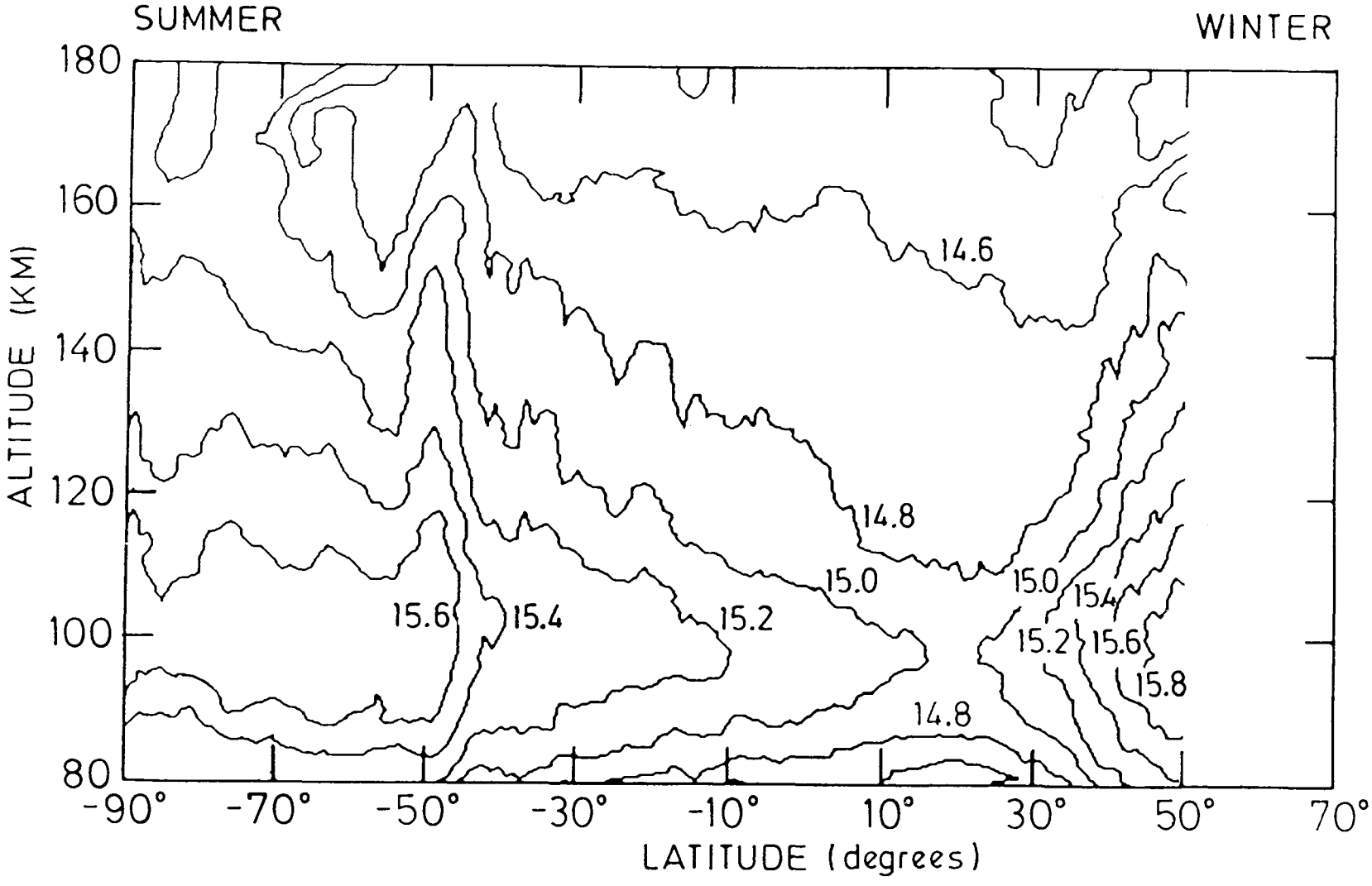

Figure 1. Log_{10} of horizontal column densities (cm^{-2}) of NO observed with the UVNO experiment on the Atmosphere Explorer-D (AE-D) satellite.

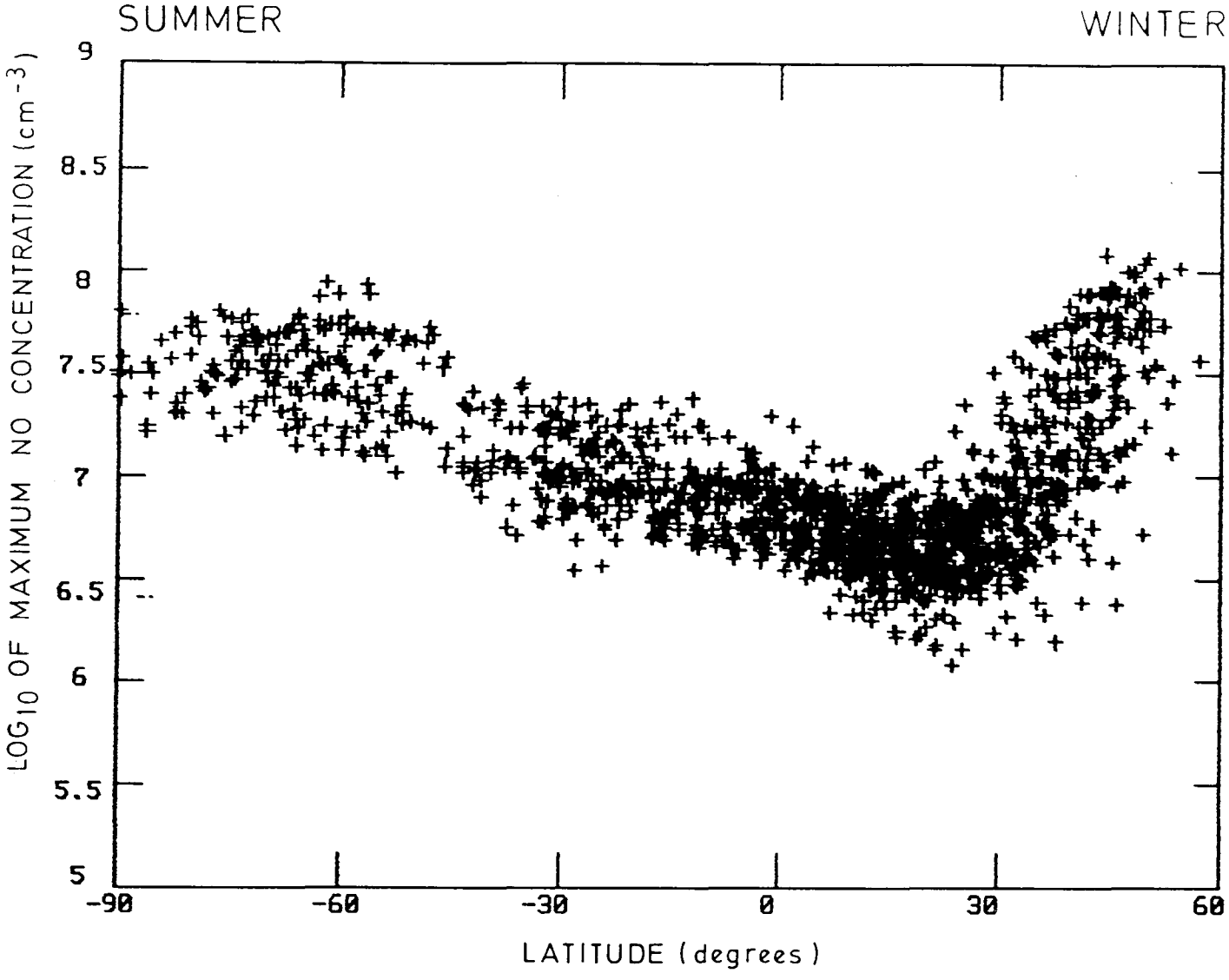

Figure 2. Latitudinal distribution of $\log_{10}$ of the NO peak concentration measured from AE-D ("spinning orbits").

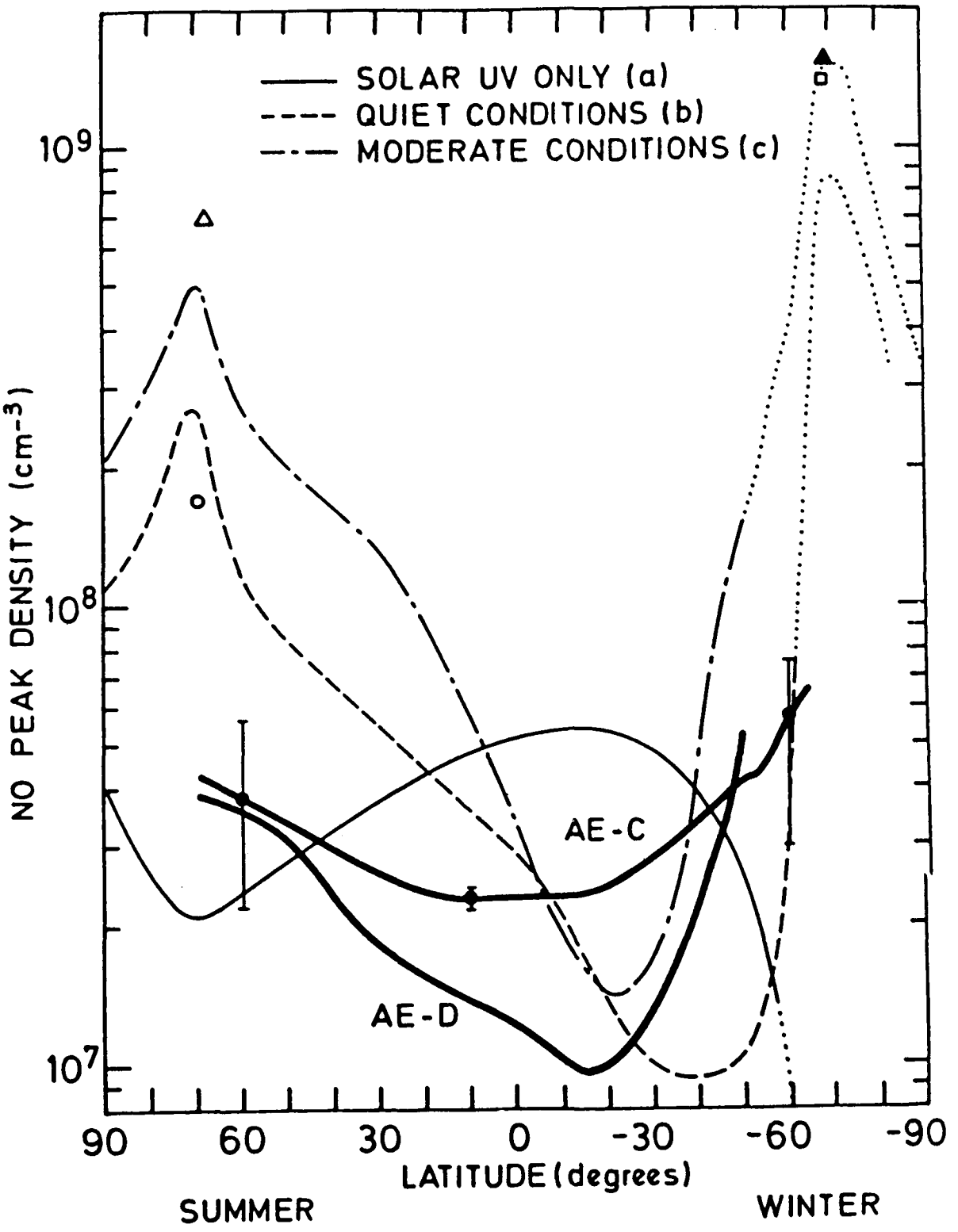

Figure 3. Comparison between NO peak densities obtained with the 2-D odd nitrogen model and AE-C, AE-D and high latitude rocket measurements.

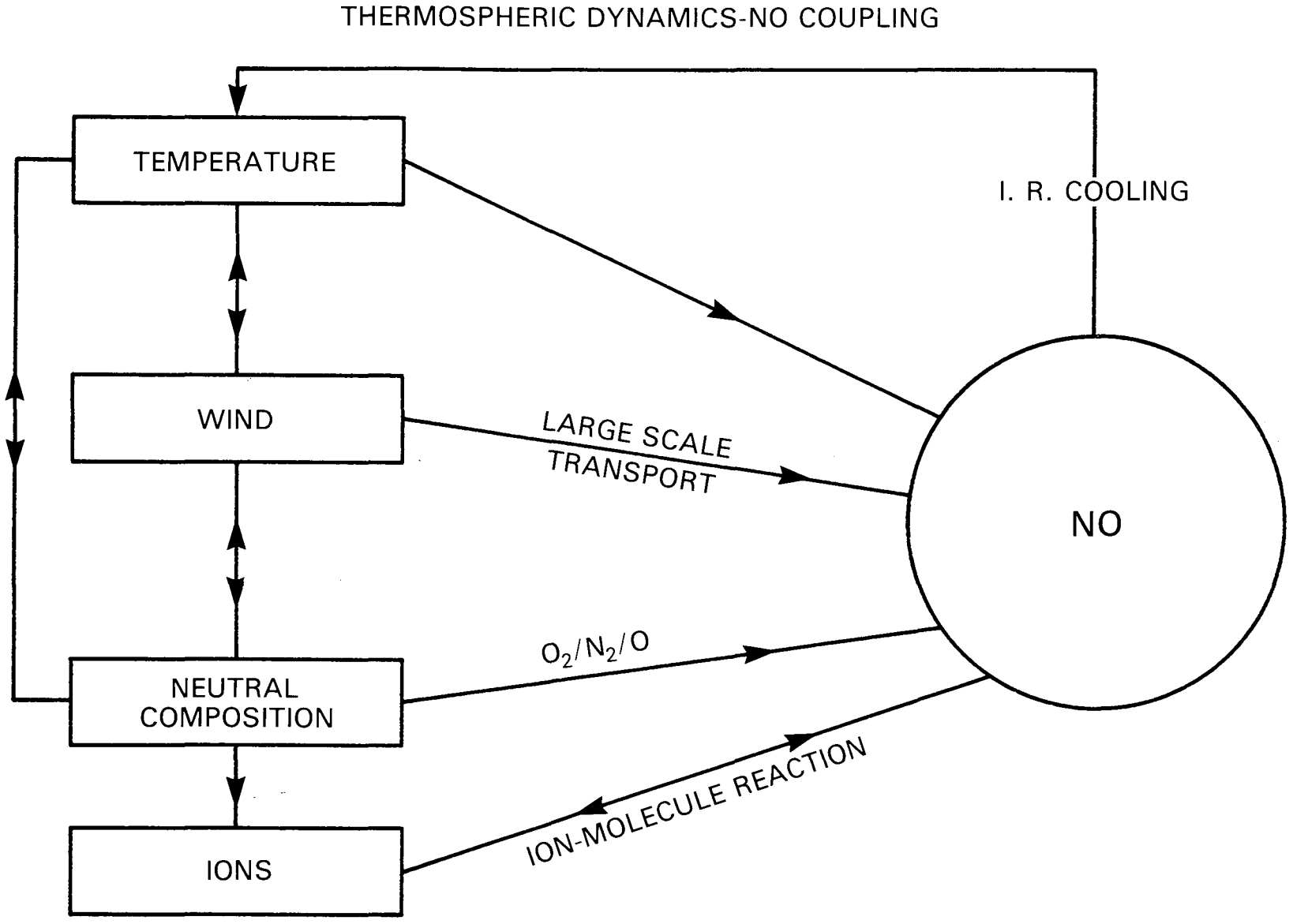

Figure 4. Block diagram of the coupling between the thermospheric structure and the nitric oxide concentration.

MODEL EQUATIONS

CONTINUITY:

$$\frac{d\rho}{dt} + \rho \, \mathrm{div} \, \vec{v} = 0$$

THERMODYNAMIC:

$$\rho c_v \frac{dT}{dt} = - \mathrm{div} \, \vec{\phi}_h - P \, \mathrm{div} \, \vec{v} + Q$$

MOMENTUM:

$$\frac{d\vec{v}}{dt} = -2\vec{\Omega} \times \vec{v} - \frac{1}{\rho} \mathrm{grad} \, P + \vec{g} + \nu \nabla^2 \vec{v} - \lambda \vec{v}$$

HYDROSTATIC:

$$\frac{\partial P}{\partial z} = - \frac{P}{H}$$

PERFECT GAS LAW:

$$P = \rho \, k \, T / \bar{m}$$

CHEMICAL:

$$\frac{\partial (n_i \, m_i \, \rho)}{\partial t} = p_i - l_i \, (n_i \, m_i \, \rho) - \mathrm{div} \, \vec{\phi}_i$$

$$\vec{\phi}_i = n_i \, m_i \, \rho \, \vec{v} + \vec{\phi}_{diff}$$

Figure 5. Equations of the 2-D model of the thermospheric structure.

NITRIC OXIDE I. R. COOLING

$$L_{NO} = h\nu\ [NO]_{v=1}\ A_{1,0}$$

$$= h\nu\ A_{1,0}\ \omega\ [NO]_{v=0}\ e^{-\frac{h\nu}{kT}}$$

WITH:

$$\omega = \frac{k_{1,0}\ [O]}{k_{1,0}\ [O] + A_{1,0}}$$

$k_{1,0}$: QUENCHING COEFFICIENT OF NO ($v=1$) BY O $\simeq 6.5 \times 10^{-11}\ cm^3 s^{-1}$

$A_{1,0} = 13.3\ s^{-1}$

Figure 6. Expression for the heat loss by NO ($v=1 \rightarrow 0$) infrared transition.

THERMODYNAMIC EQUATION

$$\frac{\partial T}{\partial t} = Q_c + Q_a + Q_{ad} + Q_{ch} + Q_s + Q_m + Q_{CO_2} + Q_{NO}$$

$$Q_c = \frac{1}{\rho c_v H_0} \frac{\partial}{\partial z}\left(\frac{K_e}{H_0} \frac{\partial T}{\partial z}\right)\text{: CONDUCTION}$$

$$Q_a = \frac{v}{r} \frac{\partial T}{\partial \theta} - \frac{w}{H_0} \frac{\partial T}{\partial z}\text{ : HORIZONTAL AND VERTICAL ADVECTION}$$

$$Q_{ad} = \frac{kT}{\bar{m}\rho c_v r} \frac{v}{r} \frac{\partial \rho}{\partial \theta} + \frac{kT}{\bar{m}\rho c_v} \frac{w}{H_0} \frac{\partial \rho}{\partial z}\text{ : ADIABATIC HEATING}$$

Q_{ch}: CHEMICAL HEATING

Q_s: SOLAR HEATING

$Q_m = Q_{particle} + Q_{JOULE} + Q_{CAP}$: MAGNETOSPHERIC HEATING

Q_{CO_2} : I. R. CO_2 RADIATION

Q_{NO} : I. R. NO RADIATION (5.3 μm)

Figure 7. Terms of the thermodynamic equation.

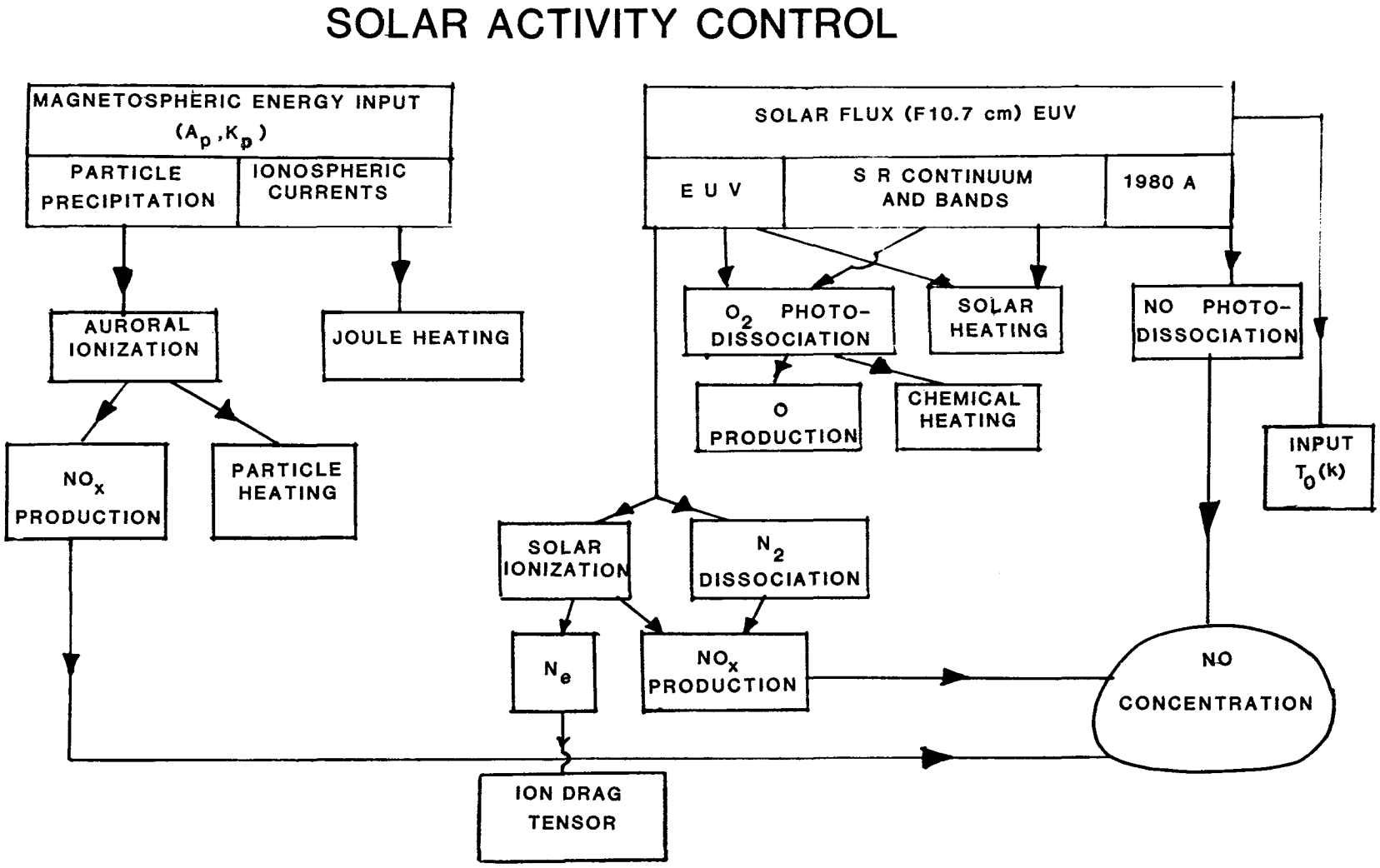

Figure 8. Block diagram showing the response of various processes in the model to solar activity.

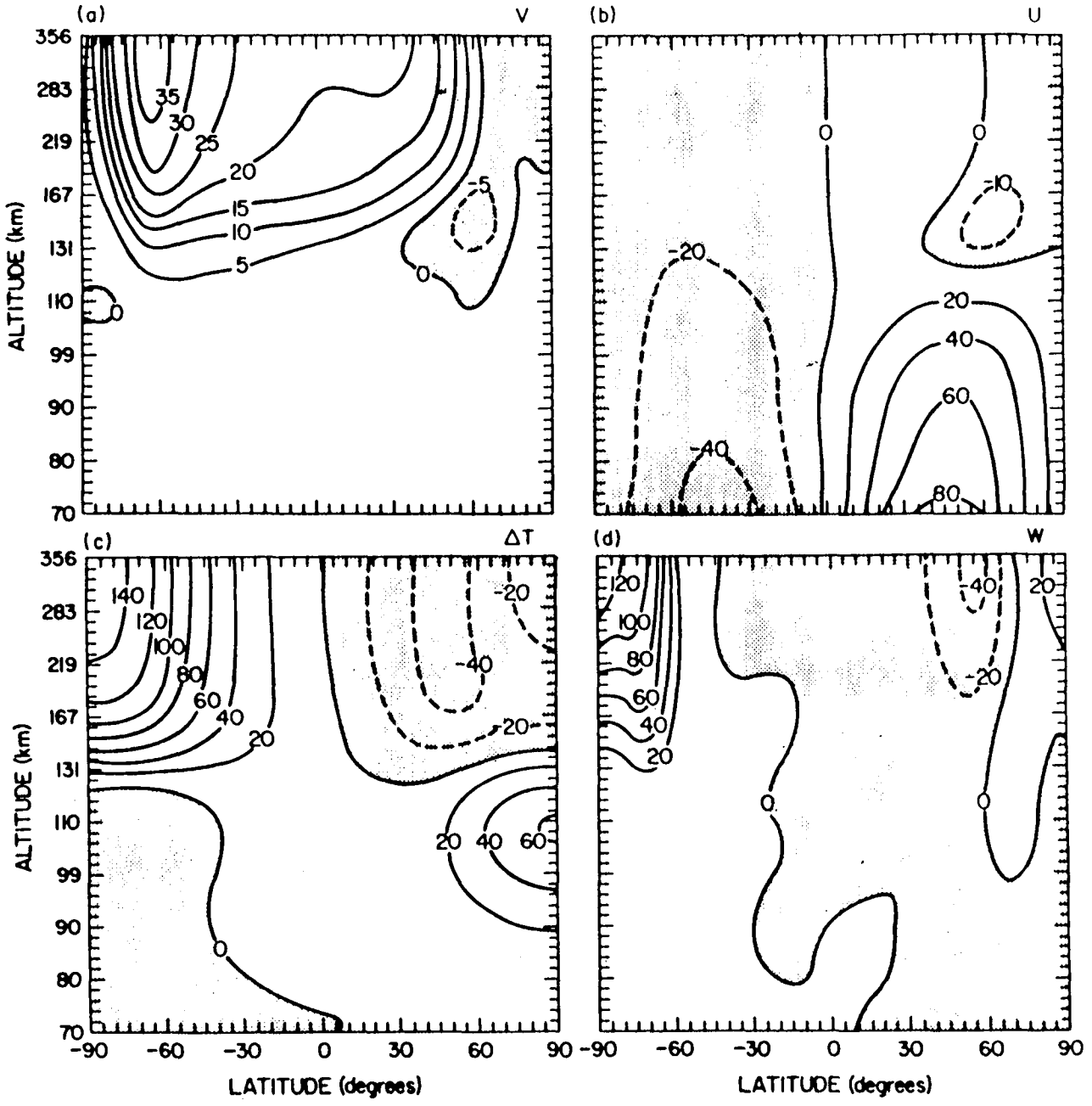

Figure 9. Contour plots of (a) the meridional wind (m.s^{-1}), (b) zonal wind (m.s^{-1}), (c) perturbation temperature (K), (d) vertical wind (cm s^{-1}) from the 2-D chemical-dynamical model.

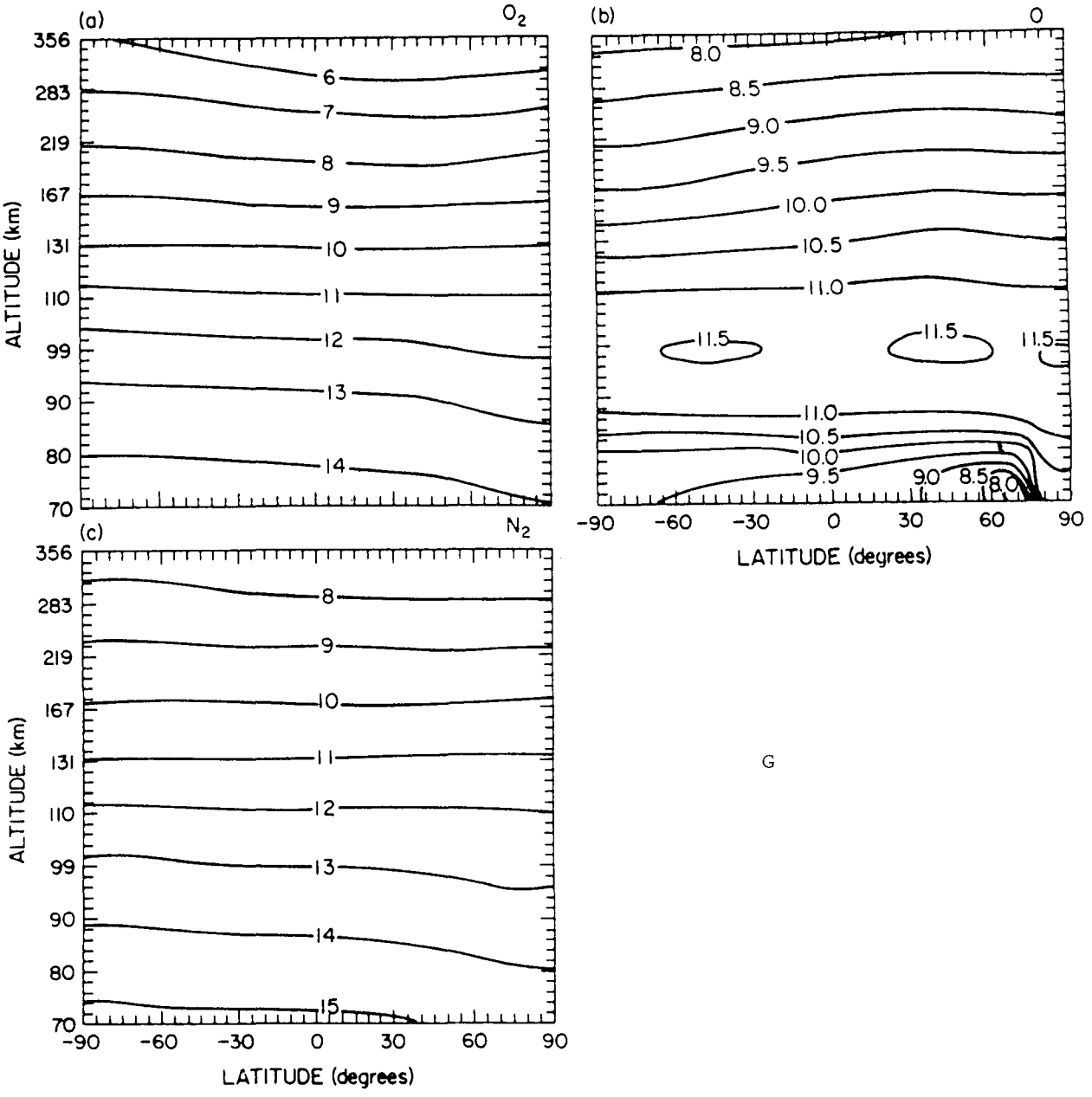

Figure 10. Contour plots of log of (a) O_2, (b) O and (c) N_2 from the 2-D dynamical-chemical model, all in cm^{-3}.

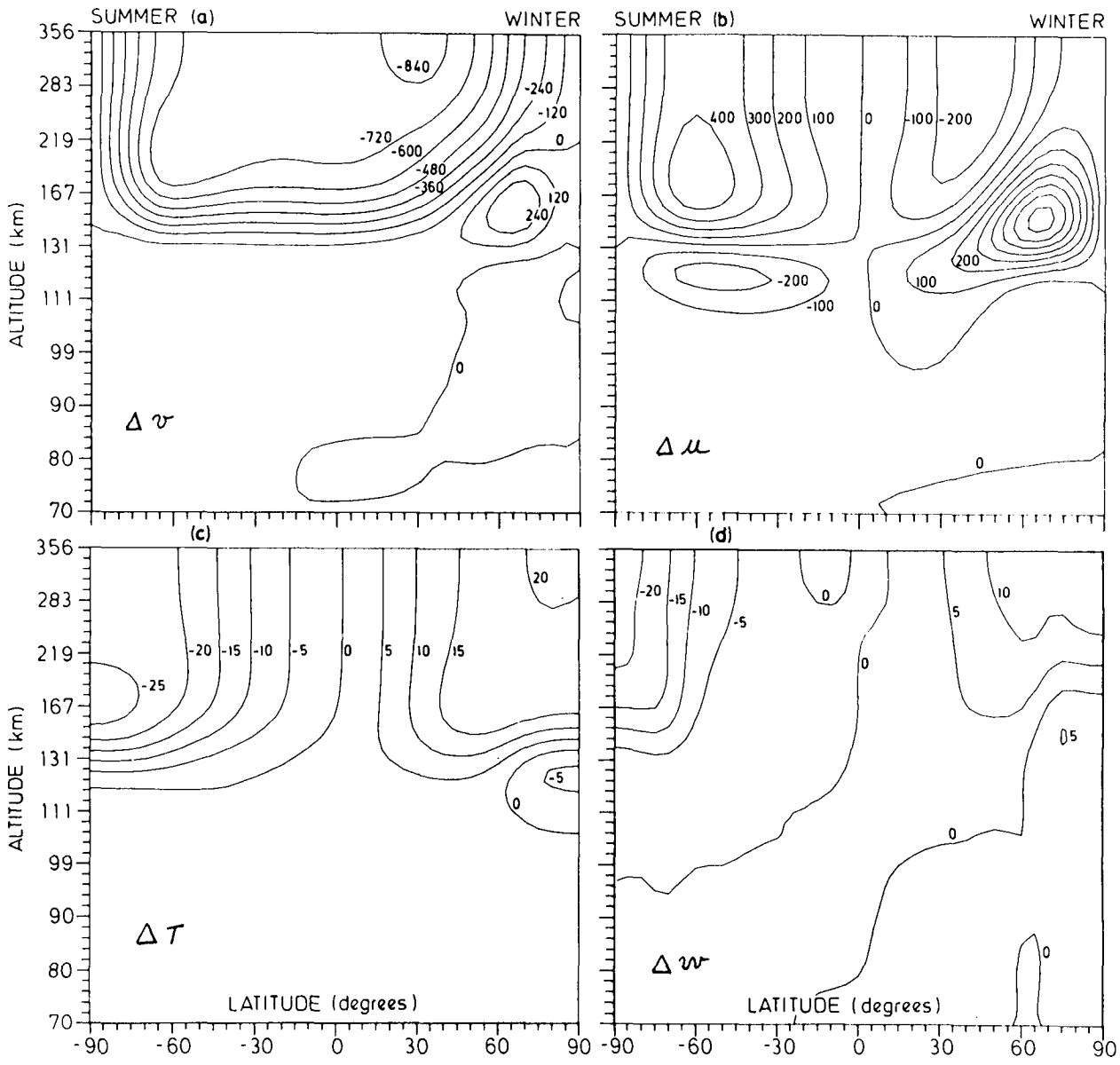

Figure 11. Contour plots of values with and without NO IR cooling for (a) meridional wind, (b) zonal wind, (c) temperature (K), (d) vertical wind. Winds are expressed in cm.s^{-1}.

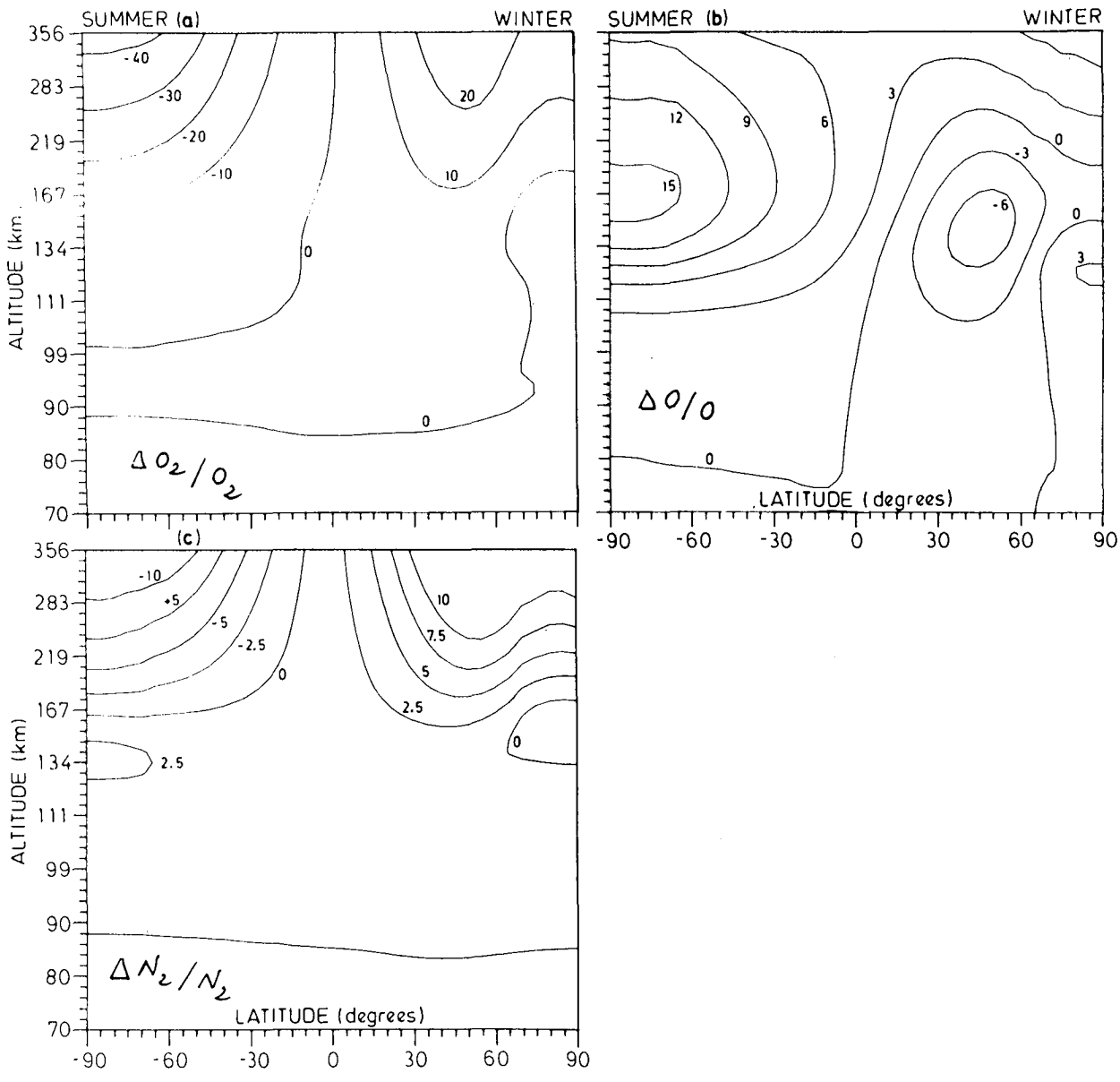

Figure 12. Contour plots displaying percentage variations of (a) O_2, (b) O and (c) N_2 when model calculations including NO IR cooling are compared to those without NO IR cooling.